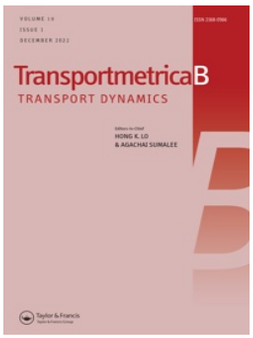

Taylor & Francis
Taylor & Francis Group

Transportmetrica B: Transport Dynamics

ISSN: (Print) (Online) Journal homepage: www.tandfonline.com/journals/ttrb20

Empirical analysis of dilemma zone using high-resolution event data

Pramesh Pudasaini, Henrick Haule & Yao-Jan Wu

To cite this article: Pramesh Pudasaini, Henrick Haule & Yao-Jan Wu (2024) Empirical analysis of dilemma zone using high-resolution event data, Transportmetrica B: Transport Dynamics, 12:1, 2379376, DOI: 10.1080/21680566.2024.2379376

To link to this article: https://doi.org/10.1080/21680566.2024.2379376

TRANSPORTMETRICA B: TRANSPORT DYNAMICS
2024, VOL. 12, NO. 1, 2379376
https://doi.org/10.1080/21680566.2024.2379376

Taylor & Francis
Taylor & Francis Group

Empirical analysis of dilemma zone using high-resolution event data

Pramesh Pudasaini, Henrick Haule and Yao-Jan Wu

Department of Civil and Architectural Engineering and Mechanics, The University of Arizona, Tucson, AZ, USA

ABSTRACT

The dilemma zone (DZ) has been physically characterized based on two divergent definitions: Type I and Type II. However, treating DZ differently based on these definitions may lead to inaccurate results of DZ boundary and subsequent safety analyses. Moreover, an integrated empirical assessment of Type I and Type II definitions for consistency in boundary quantification is not yet well-addressed. To this end, we empirically analyzed the two DZ definitions by comparing their boundary dynamics with approach velocity and time of day. First, we proposed a rule-based matching methodology with 92% accuracy to match actuation events between the advance and stop-bar detectors. This methodology was then applied to process two months of high-resolution event data from an intersection approach, yielding 28,700 vehicle arrivals on yellow. Results showed that 13.2% of approaching vehicles fall into an indecision zone or make Type I-contrary stop/run decisions at the yellow onset. The Type I and Type II DZ boundaries were temporally segregated and did not significantly overlap. Our novel findings indicate a lack of consistency in quantifying DZ and emphasize a need for data-driven quantification of the DZ boundary and its dynamics.

ARTICLE HISTORY
Received 1 November 2023
Accepted 8 July 2024

KEYWORDS
Dilemma zone; boundary dynamics; high-resolution event data; matching detection events; signalized intersection; detectors

Introduction

Drivers often face a dilemma as to whether they should stop or cross when presented with the yellow indication at intersections. This dilemma has been physically characterized by a zone or portion of the road segment upstream of the intersection using two definitions: the Type I and Type II dilemma zones (DZ). An integrated empirical assessment of these two types for consistency is not well-addressed in the existing literature, making the consistency check and correct quantification of DZ important for accurate analyses of signal timing parameters, detector placement, and driver's stop/run decisions at the yellow onset.

Figure 1 summarizes approaches in the existing literature to quantify Type I and Type II DZ. According to the Type I definition–based on the concept proposed by Gazis, Herman, and Maradudin (Gazis, Herman, and Maradudin 1960) and known as the GHM model–vehicles at yellow onset cannot safely stop before the stop line or cross the intersection during the yellow interval. The Type I definition also recognizes an option zone upstream of the intersection where vehicles can safely stop or go. The location of Type I DZ and option zone for any vehicle is determined based on the minimum stopping distance, the maximum clearing distance, and the vehicle's position at yellow onset. Dependency

CONTACT Pramesh Pudasaini pramesh@arizona.edu Department of Civil and Architectural Engineering and Mechanics, The University of Arizona, 1209 E 2nd St, Tucson, AZ 85721, USA

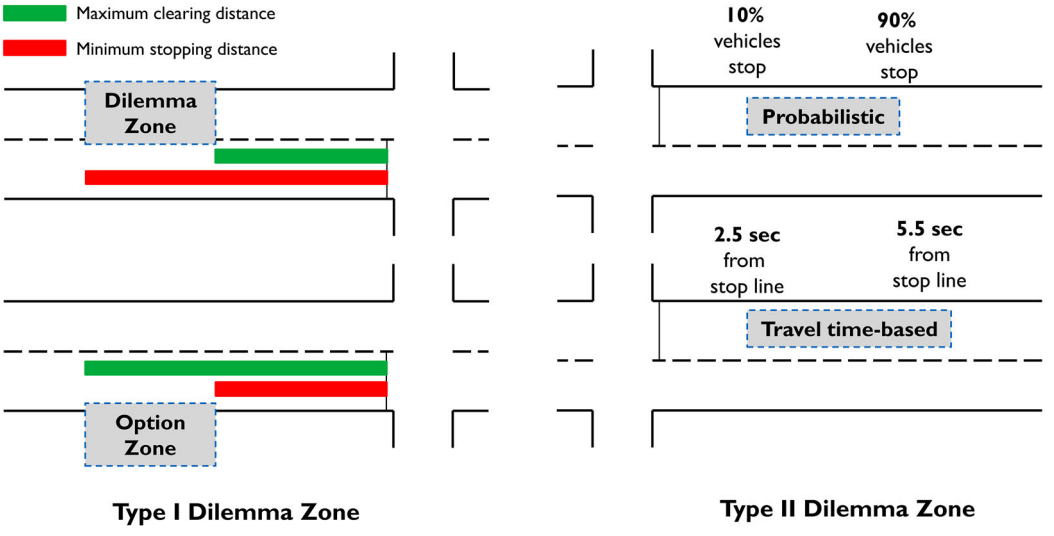

Figure 1. Quantification of Type I and Type II dilemma zones.

on such deterministic parameters for quantifying the Type I DZ is a major drawback because perfect assumptions or a priori knowledge of these parameters are required (Sharma, Bullock, and Peeta 2011; Wei et al. 2011). Moreover, Type I DZ is based on laws of physics and parameters, necessitating vehicle-specific attributes that are difficult to estimate in practice.

The Type II DZ, labeled so by Urbanik and Koonce (2007), is an 'indecision zone' at an intersection approach and is quantified via two approaches: (a) the probabilistic method by Zegeer and Curba Deen (1978) and (b) the travel time-based method by Chang, Messer, and Santiago (1985). Zegeer and Curba Deen (1978) characterized this indecision zone as the approach where between 10% and 90% of vehicles choose to stop at the yellow onset. Studies have quantified the travel time-based DZ with a rule of thumb: the location before the intersection stop-bar where the travel time is between 2.5 and 5.5 sec (Zhang, Fu, and Hu 2014; Bonneson et al. 2002; Kang, Rahman, and Lee 2020). The Type II DZ boundary quantified by a probabilistic method was constant despite varying approach velocities (Rahman, Kang, and Biswas 2021). Moreover, past studies reported a significant variation in DZ boundary for such probabilistic quantification (Sharma, Bullock, and Peeta 2011). Similarly, the travel time-based Type II definition–generalized in terms of the time to intersection stop line–does not account for the imprecision with which drivers perceive measures such as speed and distance at the yellow onset (Hurwitz et al. 2012).

Given the two divergent definitions to quantify DZ and their limitations, an integrated empirical assessment of both types for consistency is lacking in the existing literature. Zhang, Fu, and Hu (2014) point out that treating Type I and Type II DZ boundaries differently–as done in existing studies–may lead to inaccurate results of DZ-related and subsequent safety analyses. When defined based on distance from the stop line, there is also a potential overlap between the Type I and Type II DZ (Zhang, Fu, and Hu 2014). However, this potential overlap is still unexplored in existing literature. This study's primary focus and contribution is an integrated empirical analysis of the four DZ quantifications: Type I DZ, Type I option zone, Type II probabilistic DZ, and Type II travel time-based DZ. To this end, we propose a novel model using a large dataset of high-resolution event data for matching detection events between the stop-bar and advance locations to estimate the parameters of the Type I definition. This model also contributes to existing literature by advancing the use of high-resolution events data to estimate individual vehicle parameters to characterize the Type I DZ physically. In addition, this study–for the first time–assesses the variation and overlap in Type I and II DZ by approach velocity and time of day to explore the dynamic nature of the zones' boundaries.

The remainder of this paper is structured as follows. The Literature Review section summarizes prior studies on dilemma zone analysis. The Data Collection section introduces the study site and high-resolution event data. The following section presents data processing, a rule-based methodology for matching detection events, and a performance assessment of this methodology. Analysis of the Type I and II approaches to quantify dilemma zones is then conducted, followed by results and discussions of the findings. Finally, the concluding remarks of this study are drawn.

Literature review

Table 1 highlights some notable studies on DZ analysis with corresponding data sources and sample sizes used for assessment. Note that the existing studies on assessing DZ have diverged into two separate paths: the Type I and the Type II definitions. The primary data sources for DZ assessment have been speed radar (Papaioannou 2007), radar-based wide area detector (Sharma, Bullock, and Peeta 2011; National Academies of Sciences and Medicine 2012), trajectory data (Wei et al. 2011), microwave radar sensors (Rahman, Kang, and Biswas 2021), and video recordings (Gates and Noyce 2010; Hurwitz

Table 1. Summary of studies on dilemma zone assessment.

Study	Focus	Location	Data source	Sample size
Papaioannou (2007)	Factors influencing drivers' behavior in Type I DZ	1 approach of T-shaped signalized intersection in Greece	Speed radar and video recordings (315 hr)	2,452 vehicles at yellow onset
Gates and Noyce (2010)	Influence of vehicle type on driver behavior in Type II DZ	6 signalized intersections in Wisconsin	Video recordings (43 hr)	1,275 vehicles in dilemma zone
Sharma, Bullock, and Peeta (2011)	Dilemma zone hazard function for Type II DZ	1 high-speed signalized intersection in Noblesville, Indiana	Radar-based wide area detector (102 days)	2,870 cars during yellow
Wei et al. (2011)	Dynamic factors for Type I DZ	4 high-speed signalized intersections in Ohio	Trajectory data extracted from video recordings (46 hr)	1,445 vehicles during yellow
Hurwitz et al. (2012)	Driver behavior in Type II DZ using fuzzy logic	5 high-speed signalized intersections in Vermont	Video recordings (510 hr)	1,900 vehicles during yellow
National Academies of Sciences and Medicine (2012)	Timing yellow and all-red intervals based on Type II DZ	83 intersection approaches from 5 US states	Video recordings (328 hr)	7,482 vehicles during yellow
Savolainen, Sharma, and Gates (2016)	Factors influencing Type II DZ	87 intersection approaches from 5 regions in the US	Video recordings and wide area detectors (3-5 hr/site)	5,121 vehicles at yellow onset
Kang, Rahman, and Lee (2020)	Type II DZ length estimation	15 high-speed, rural intersections in Alabama	Video recordings (1,500 hr)	*Not reported*
Rahman, Kang, and Biswas (2021)	Driver's stop/go behavior and DZ boundaries	1 high-speed isolated signalized intersection in Mobile, Alabama	Microwave radar sensors (14 days), high-resolution signal event data	2,495 vehicles during yellow
This study	Exploratory analysis of Type I & Type II DZ	1 signalized intersection in Phoenix, Arizona	High-resolution event data (2 months)	28,700 vehicle arrivals at yellow onset

et al. 2012; Kang, Rahman, and Lee 2020; Savolainen, Sharma, and Gates 2016). These data sources suffer from difficulties in data processing and require concurrent video recordings for validation, making it difficult to obtain a large sample size for assessing DZ boundary.

This study uses high-resolution event data to obtain a relatively large dataset of detector actuations that can be processed and analyzed for DZ assessment. High-resolution event data comprises signal phase change and detector actuation events, which has facilitated the estimation of performance measures such as queue length (Pudasaini, Karimpour, and Wu 2023), red light running severity (Jalali Khalilabadi, Karimpour, and Wu 2023), pedestrian delay (Karimpour et al. 2022), and pedestrian volume (Li and Wu 2021). For DZ analysis, however, using high-resolution event data requires a method for matching actuation events between the advance and stop-bar detectors. Existing studies using such data have adopted a window-searching-based methodology to match detection events between advance and stop-bar or stop-bar and entrance detectors (Wu et al. 2013; Lu et al. 2015; Ding et al. 2016; Ren et al. 2016; Chen et al. 2017). Some common limitations of these approaches include giving up the search for a matching pair in case of multiple matches, estimation of velocity using an a priori known effective vehicle length, exclusion of long vehicles, and exclusion of left-turning vehicles. Furthermore, to the best of the authors' knowledge, the accuracy of the matching pairs has not been reported in any of these prior studies. Hence, we propose a novel rule-based model for matching detection events between advance and stop-bar detectors in this study. The subsequent analysis of Type I and Type II DZ using a large dataset is done based on matching pairs of detector actuation events predicted by this methodology.

Data Collection

Study site

The westbound approach of Indian School Rd and 19th Ave in Phoenix, Arizona, was selected as the study site for empirical analysis of DZ. We selected this intersection for two reasons. First, Indian School Rd is one of the busiest arterials in Phoenix, providing a direct connection between the I-17 highway and the US 51 highway. In the vicinity of 19th Ave, Indian School Rd had an annual average daily traffic of 44,500 vehicles in 2022. Second, the intersection at Indian School Rd and 19th Ave was equipped with lane-by-lane loop detectors at the stop-bar and advance locations. Timestamped events data from the intersection's signal controllers–including actuations on detectors–is archived in real-time by the City of Phoenix Street Transportation Department.

Figure 2 presents the study site's westbound approach with layout and detector configuration. The approach has lane-by-lane loop detectors on three through lanes at the stop-bar and advance locations. The left-turn lane has front and rear detectors. Advance detectors are 5 ft (1.5 m) long, whereas stop-bar detectors are 40 ft (12.2 m) long. The distance between the stop line and the advance detector is 300 ft (91.4 m). The speed limit of the approach is 35 mph (56 km/hr).

High-resolution event data

High-resolution event data in the form of timestamped events from the signal controller and detectors were collected from TransSuite, a centralized traffic management system archiving real-time data from the City of Phoenix intersections. Timestamped events comprise signal phase changes, detector actuations, and communication attempts at a resolution of 0.1 sec. The signal phase change events contain each phase's start and end times of green, yellow, and red intervals. The detector actuation events contain the timestamp at which a vehicle actuated a detector 'on' and 'off.' Similarly, the communication attempt events contain information on communication loss in the signal controller, making this dataset useful to assess potential loss in signal phase changes and detector actuations during a specific period.

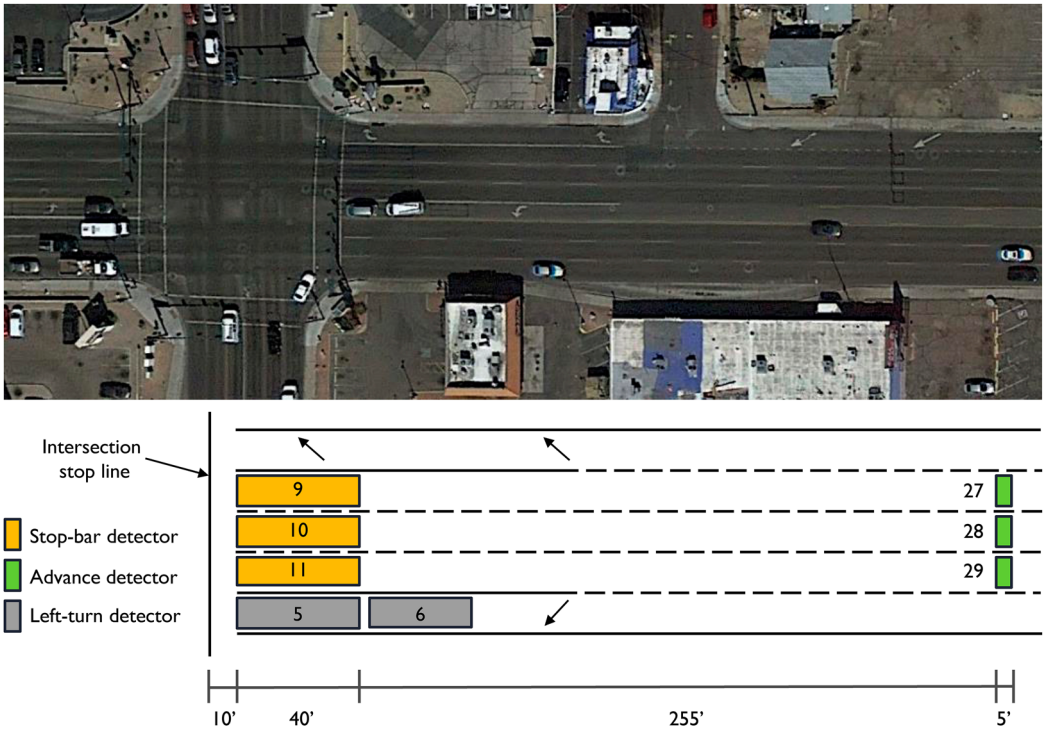

Figure 2. Study intersection with detector layout and configuration (source: Google Earth, 2023).

This study divided the available high-resolution events datasets into two groups. The first dataset, collected for 7 hours from three weekdays (6/12/2022, 6/14/2022, 3/27/2023), had concurrent ground-truth video recordings available in the TransSuite system. The availability of both event datasets and concurrent videos made this dataset suitable to assess the performance of the proposed rule-based model for matching actuation events between the stop-bar and advance detectors. The second dataset, used for analyzing DZ, was collected throughout January and February 2023. Details of processing these high-resolution event data are presented in the following section.

Matching detection events

Figure 3 outlines the overall framework and methodological steps in this study. Following site selection and high-resolution event data collection, the data is processed, and actuations at the yellow onset are filtered. Next, a Rule-based Algorithm for Matching Detections (RAMD) is proposed and tested for matching detection events between the advance and stop bar detectors. The RAMD yields pairs of matched vehicle detections. Each pair represents a single vehicle, with one detection each at the advance and the stop bar detector locations. By analyzing these detection pairs, the travel time for each vehicle from the advance detector to the stop bar is calculated. Finally, the parameters of Type I DZ and boundaries for each DZ quantification model are computed and compared.

The following sections discuss the data processing framework and the proposed rule-based model for matching actuation events. As shown in Figure 4, the overall data processing was carried out in three steps: pre-processing raw high-resolution event data, processing signal phase change and detector actuation events, and filtering actuation events at yellow onset. Then, the rule-based model is proposed, and its performance evaluation is conducted before applying the data processing framework and the model to the large dataset for DZ analysis.

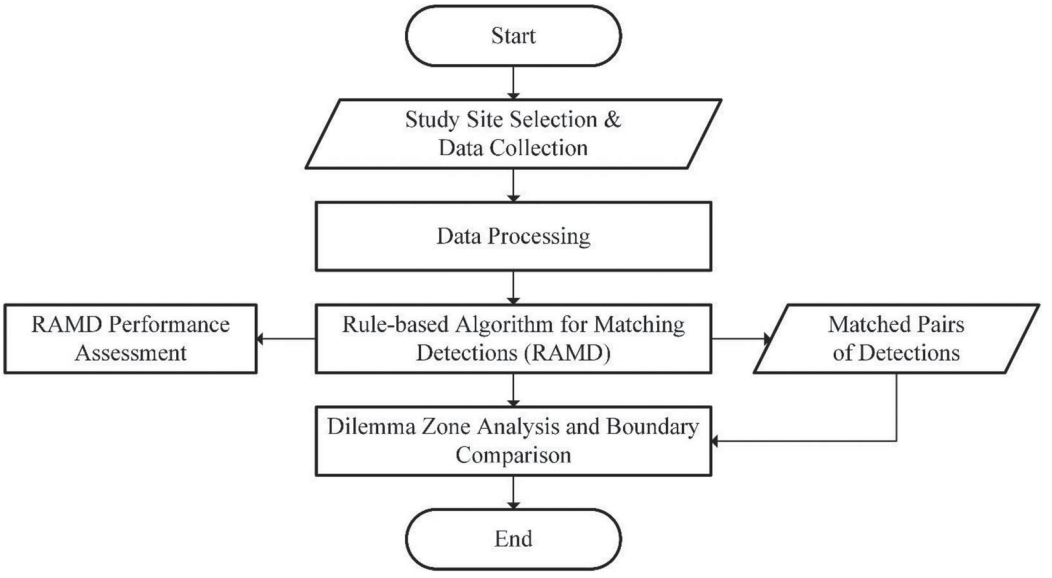

Figure 3. Study Framework.

Data Processing

The available dataset was first segregated into individual hours for data pre-processing. An assessment of communication loss and a visual check of data continuity plots for signal phase changes and detector actuation provided a data quality check for further processing. The signal phase change events and detector actuation events datasets were loaded, and parameters of interest were computed for hourly datasets without communication loss.

Table 2 lists the indices, sets, and parameters used throughout this study. With signal phase changes, the timestamps of yellow (T_c^y), red (T_c^r), and green (T_c^g) indications for each cycle along with the minimum and maximum cycle start and end times (the first and last yellow indication in the hour) were stored. Each cycle was assumed to start on the yellow indication for data processing. Then, the detector actuation events were filtered to include only the actuations within the minimum and maximum limits of cycle start times.

The signal phase changes and detector actuation datasets were merged, and the dataset was split for computing actuation parameters on each through lane. Let T_i^o and T_i^f be the timestamps of actuations 'on' and 'off' for each detector. Occupancy time (τ_i^D), headway (τ_i^H), and gap (τ_i^G) as defined by Eq. (1), (2), and (3), respectively, were computed for actuations on each detector. Next, the signal change during actuation ($SCA_i \in \{YY, YR, RR, RG, GG, GY\}$) is introduced as an important parameter denoting a combination of the changes in signal indication when a particular actuation is turned 'on' and 'off.' For instance, $SCA_i \in \{GG\}$ indicates that actuation i started on the green indication and ended on the green; $SCA_i \in \{RG\}$ indicates that actuation i started on the red indication and ended on the green. Pudasaini, Karimpour, and Wu (2023) found that SCA_i when used in conjunction with occupancy time yields accurate information about a vehicle's stop/run decision over a detector. In general, $SCA_i \in \{GG\}$ have a low occupancy time, implying that vehicles corresponding to such actuations crossed the detector. The most useful case is $SCA_i \in \{RG\}$, which usually has a high occupancy time, meaning such actuations correspond to vehicles actuating the detector on red, stopping before the stop line, and leaving the detector on the green; in other words, these vehicles stopped over the stop bar. Hence, a vehicle i's stop/run decision can be accurately known using the combination of signal change during actuation and occupancy time parameters. For a detailed overview and empirical analysis of SCA_i with

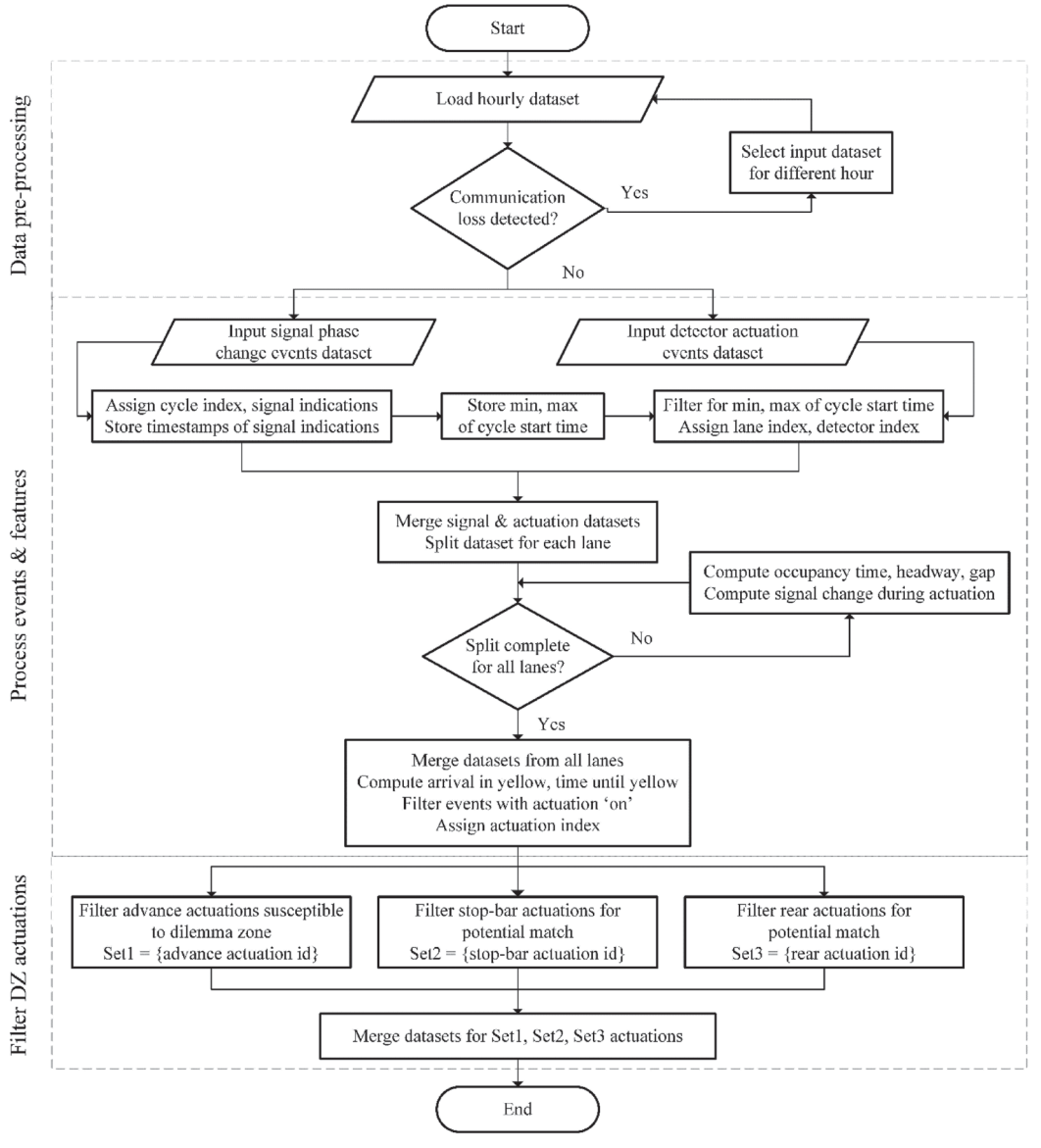

Figure 4. Data processing flowchart.

respect to τ_i^D, τ_i^H, and τ_i^G parameters, interested readers are referred to Pudasaini, Karimpour, and Wu (2023).

$$\tau_i^D = T_i^f - T_i^o \qquad \forall i \tag{1}$$

$$\tau_i^H = T_{i+1}^o - T_i^o \qquad \forall i \tag{2}$$

$$\tau_i^G = T_{i+1}^o - T_i^f \qquad \forall i \tag{3}$$

Upon computation of parameters, the datasets are merged again for all through lanes. For each actuation, the arrival in yellow (AIY) of the current cycle and the time until yellow (TUY) of the next cycle are computed using equations (4) and (5), respectively. Since the focus is on DZ analysis, for

Table 2. Notations used in this study.

Notation	Description
Indices	
i	Vehicle or detector actuation
c	Cycle
o, f	Detector 'on' and 'off' events
y, r, g	Yellow, red, and green indication events
Sets	
SCA	Signal change during actuation for vehicle i; $SCA \in \{YY, YR, RR, RG, GG, GY\}$
Parameters	
T_c^y, T_c^r, T_c^g	Timestamp of yellow, red, and green indications for cycle c
T_i^o, T_i^f	Timestamp of actuation 'on' and 'off' for vehicle i
τ_i^D	Occupancy time for actuation i (sec)
τ_i^H	Time headway between detector actuation i and $i+1$ (sec)
τ_i^G	Time gap between detector actuation i and $i+1$ (sec)
AIY_i, AIY_i'	Arrival in yellow of actuation i at advance and stop-bar detectors (sec)
TUY_i, TUY_i'	Time until yellow of actuation i at advance and stop-bar detectors (sec)
AIY_{crit}, AIY_{crit}'	Critical arrival in yellow of actuation i at advance and stop-bar detectors (sec)
TUY_{crit}, TUY_{crit}'	Critical time until yellow of actuation i at advance and stop-bar detectors (sec)
γ	Yellow interval of intersection (sec)
$t_{min}', t_{max}', t_{ideal}'$	Minimum, maximum, and ideal travel time for actuation i to travel from advance detector to rear detector (sec)
t_{min}, t_{max}	Minimum and maximum travel time for actuation i to travel from advance detector to stop-bar detector (sec)
$t_{ideal}^{stop}, t_{ideal}^{run}$	Ideal travel time from advance detector for actuation i to stop at or run over stop-bar detector (sec)
V_i	Approach velocity of vehicle i between advance and stop-bar detectors (ft/sec)
t_i	Travel time of vehicle i between advance and stop-bar detectors (sec)
D'	Distance between the rear ends of advance and stop-bar detectors (ft)
D	Distance between intersection stop line and rear end of advance detector (ft)
d	Distance between intersection stop line and rear end of stop-bar detector (ft)
X_i^p	Position of vehicle i from the intersection stop line at yellow onset (ft)
δ_i	Perception-reaction time of vehicle i (sec)
a_i^{stop}	Deceleration rate of vehicle i stopping at the stop line (ft/s^2)
a_i^{run}	Acceleration rate of vehicle i running over the stop line (ft/s^2)
V_{85}	85th percentile speed of intersection approach (ft/sec)
α_i	Binary variable for stop/run decision of vehicle i
a_{crit}^{stop}	Maximum deceleration for running vehicles (ft/s^2)
a_{crit}^{run}	Maximum acceleration for stopping vehicles (ft/s^2)
X_i^s	Minimum stopping distance for vehicle i (ft)
X_i^c	Maximum clearing distance for vehicle i (ft)

vehicles actuating a detector after the indication turns yellow, AIY indicates the passage of the yellow indication time at which a vehicle arrived at the detector. Conversely, TUY indicates the time left until the yellow indication of the next cycle begins. In the final step of processing events, the dataset is filtered for all events with the actuation 'on.' Here, we combine the through-lane actuation events with the actuation 'on' events on the left-turn lane. Additionally, all actuation events are assigned an actuation index.

$$AIY_i = T_i^o - T_c^y \qquad \forall i \tag{4}$$

$$TUY_i = T_{c+1}^y - T_i^o \qquad \forall i \tag{5}$$

Once processing of high-resolution events is complete, the final step of data processing is filtering out potential actuations susceptible to DZ. At the advance location, we filter actuations with $AIY_{crit} \leq \gamma$ or $TUY_{crit} \leq t_{ideal}$, where $\gamma = 3.6$ is the duration of the yellow interval and $t_{ideal} = 6$ is the approximate ideal travel time from the advance detector to the intersection stop line at the speed limit, i.e. traveling 310 ft (94.5 m) at 35 mph (56.3 km/hr). This filtering ensures that all vehicle arrivals at the yellow onset from the intersection stop line to a point beyond the advance location are captured. The filtering parameters at the stop-bar detectors were SCA, AIY, and TUY. All SCA except 'GG' and actuations with higher AIY were filtered out at the stop-bar, as vehicles corresponding to these actuations were

not subject to DZ when crossing the intersection stop line. Further, actuations with $AIY'_{crit} \leq 12$ or $TUY'_{crit} \leq 1.5$ were retained as the potential matches for actuations filtered at the advance location. $AIY'_{crit} \leq 12$ at the stop-bar location ensures potential matches for vehicles that decelerate downstream of the advance location and decide to stop before the intersection stop line. $TUY'_{crit} \leq 1.5$ is for stop-bar actuations that face the yellow onset between the intersection stop line and the rear of the stop-bar detector. Finally, the three sets of detector actuation indices with their corresponding features in the merged dataset were passed to the rule-based model for matching detections between the advance and stop-bar detectors.

Rule-based Algorithm for Matching Detections (RAMD)

We manually verified the matches from video recordings available for 7 hours to obtain a ground-truth match of actuations between the stop bar and advance locations. Since each vehicle in the final dataset obtained from data processing was assigned an actuation index, the objective was to get paired sets of actuation matches between (a) advance and left-turn rear detector and (b) advance and stop-bar detector. The proposed rule-based model relies on a set of minimum and maximum values of travel time that–for each advance actuation–constrains the search space for a set of stop-bar actuations.

Matching Left Lane Advance Actuations with Left-Turn Lane Rear Actuations

We assume that vehicles changing lanes to the left-turn lane do so only from the left-most through lane, as we found no vehicle changing lanes to the left-turn lane from the middle through lane. From observation of available videos by a trained individual, we observed approximately 14% of actuations on the left lane's advance detector opting to take a left turn at the intersection. Hence, the first step is to match the actuations on the left lane's advance detector with those on the left-turn lane's rear detector. The travel time from the left lane's advance detector to the left-turn lane's rear detector was analyzed based on 20 sample matches verified from videos. Table 3 summarizes the descriptive statistics of the travel time between verified actuation matches at the left-turn advance detector and rear detector. The minimum (t'_{min}) and maximum (t'_{max}) values of travel time for limiting the search space for the set of rear actuations were taken as 4 sec and 7 sec, respectively. Similarly, the ideal travel time (t'_{ideal}) of 5.3 sec was chosen based on the mean travel time for computing the strength of a matching pair. The matching strength between a match pair is the inverse of the difference between the travel time between the pairs and t'_{ideal}. The rule-based algorithm for matching detections (RAMD) between the advance and the rear locations is presented in Table 4. In cases where multiple match cases of advance actuation are found for a rear actuation index, the matching pair with the highest matching strength is selected. The final output is a set of actuations on the left lane's advance detector that take a left turn

Table 3. Descriptive statistics of travel time between video-verified detection matches

		Advance to stop-bar detector	
Parameters	Left-lane advance to rear detector	Stopping	Running
Sample size	20	143	160
min	4.60	4.40	3.10
25th percentile	4.90	5.80	4.00
median	5.30	6.50	4.50
mean	5.34	6.58	4.63
75th percentile	5.70	7.20	5.03
max	6.50	10.10	8.00
95% confidence interval	[5.07, 5.61]	[6.4, 6.75]	[4.5, 4.76]

Table 4. Rule-based algorithm for matching detection events.

Start
Input dataset: final processed dataset
Input actuation sets: advance (S), stop-bar (S'), and rear (S'') actuations
Input parameters: $t'_{min}, t'_{max}, t'_{ideal}, t_{min}, t_{max}, t^{stop}_{ideal}, t^{run}_{ideal}$
Initialize: vectors to contain initial match pairs (M) and final match pairs (M')
// match actuations between advance and rear detectors
For i in S **do**
  Initialize: vector to contain candidate match pairs (C)
  For k in S'' **do**
    $t'_{ik} = T'_k - T_i$ *// travel time between i and k actuations*
    If $t'_{min} \leq t'_{ik} \leq t'_{max}$
      $MS_{ik} = 1/(t'_{ik} - t'_{ideal})C[k] = [k, MS_{ik}]$ *// append vector of rear actuation index and matching strength toC*
      $C[k] = [k, MS_{ik}]$ *// append vector of rear actuation index and matching strength toC*
  End Loop
  If C is not null *// potential match pair found for advance-rear actuations*
    $M'[i] = C[k]$
// process $M'[i]$ to select the highest matching pairs and get set S_i with rear actuation matches
$S = S - S_i$ *// update advance set to exclude rear set matches*
// match actuations between advance and stop-bar detectors
For i in S **do**
  Initialize: vector to contain candidate match pairs (C)
  For j in S' **do** *// set of stop-bar actuations on the same lane*
    $t_{ij} = T_j - T_i$ *// travel time between i and j actuations*
    If $t_{min} \leq t_{ij} \leq t_{max}$
      If $\alpha_i = 0$ *// decision to stop*
        $MS_{ij} = 1/(t_{ij} - t^{stop}_{ideal})$
      Else // decision to run
        $MS_{ij} = 1/(t_{ij} - t^{run}_{ideal})$
      $C[j] = [i, MS_{ij}]$ *// append vector of advance actuation index and matching strength toC*
  End Loop
  If C is not null *// potential match pair found for advance-stop-bar actuations*
    $M'[i] = C[k]$
// process $M'[i]$ to select the highest matching pairs and get set match pairs (S', S)
End

to the rear detector. This set of rear actuations can now be removed while matching actuation events between advance and stop-bar detectors.

Matching Advance Actuations with Stop-bar Actuations

From observation of available videos by a trained individual, the actuations on the advance detector were matched with that on the stop-bar detector. Of 303 matches identified between the advance and stop-bar detectors at yellow onset, 160 vehicles decided to run through the intersection stop line, whereas the remaining 143 decided to stop. Of the 160 running cases, 113 vehicles were yellow light runners (YLR), whereas the remaining 47 were red light runners (RLR). We also segregated the matches based on whether the vehicles were car-following at the advance location. Brackstone and McDonald (1999), in their comprehensive historical review of car-following, identified a commonly used threshold of 1.5 s for time headway to define car-following. Based on this limit of car-following, 61 out of 242 samples were observed to be following the leading vehicle at the advance location. We selected car-following, stop/run decisions, and YLR/RLR decisions from the dataset of manually verified matches as the rules for building a rule-based model.

The robustness of a rule-based decision tree model was assessed based on three t-tests. The Shapiro–Wilk normality test provided evidence for the normality of each t-test. Welch's two-sample t-test at 0.05 level (p-value $= 0.1982$) failed to reject the null hypothesis that the true difference in means between the car-following and non-car-following groups is zero. Thus, we discard the car-following decision from our rule-based model. The second t-test at 0.05 level (p-value ≈ 0) failed to provide evidence for the null hypothesis that the true difference in means of travel time between stopping

and running vehicles is zero. Finally, a t-test at 0.05 level (p-value = 0.5011) failed to reject the null hypothesis that the true difference in means of travel time between RLR and YLR equals zero.

We finalize stopping and running vehicles as two separate groups based on statistical tests conducted for the abovementioned groups. Table 3 summarizes the descriptive statistics for travel time for stopping and running video-verified matches between advance and stop-bar locations. The minimum (t_{min}) and maximum (t_{max}) values of travel time for limiting the search space for a set of stop-bar actuations were taken as 3 sec and 11 sec, respectively. Similarly, the ideal travel times for stopping (t_{ideal}^{stop}) as 6.6 sec and for running (t_{ideal}^{run}) as 4.6 sec were chosen based on their respective mean travel times. The RAMD model for advance and stop-bar locations is continued in Table 4. If multiple match cases of advance actuation index are found for an actuation index at the stop-bar detector, the algorithm selects the matching pair with the highest matching strength.

Model performance assessment

The accuracy of the proposed RAMD model was assessed by comparing the match pairs predicted by the RAMD model with the ground-truth match pairs noted from video observations. We used precision, recall, and the F1 score to quantitatively assess accuracy. The model produced 100% precision and 95.2% recall for the match pairs between advance and rear detectors. For the match pairs between advance and stop-bar detectors, the model yielded a precision of 92% and a recall of 91.1%. Such high accuracy in terms of precision and recall indicates that the proposed RAMD model produces low false alarms and misses a small proportion of the actual match pairs during prediction.

The performance of the RAMD model was compared with two other commonly used methods for matching detection events between advance and stop-bar locations. The two methods, called hereafter 'Ding's method' and 'Lu's method,' were based on a time window for each actuation at the advance location, with velocity computed as a function of a known effective vehicle length (Ding et al. 2016; Lu et al. 2015). The respective studies did not report the accuracies of the match pairs predicted by these methods. Moreover, long vehicles were discarded in Lu's analysis due to the assumption of an effective vehicle length. Here, we compare the proposed RAMD model with Ding's and Lu's methods and conduct a sensitivity analysis. As presented in Figure 5, the comparison based on precision, recall, and F1 scores demonstrates the superiority of the proposed RAMD model, unaffected by the assumption of an effective vehicle length. Figure 5 also shows that the transferability of Ding's and Lu's method to other intersections is subject to a priori knowledge of effective vehicle length, as an incorrect assumption of this parameter can heavily skew the accuracy of match pairs.

Next, the sensitivity analysis of the proposed RAMD model was assessed for two critical parameters used in the model: (a) the ideal travel time for running and (b) the ideal travel time for stopping. As presented in Figure 6, the analysis was carried out with the F1 score as the metric. We observed that the highest F1 score corresponded to (a) 6.6 sec for stopping and 4.6 sec for running, and (b) 6.7 sec for stopping and 4.6 for running. Since the ideal travel time values for stopping and running in the RAMD model were assessed based on sound statistical tests, we observe that the chosen ideal travel time values corresponded to the highest F1 score. Figure 5 and Figure 6 demonstrate that the proposed RAMD model is robust in terms of assumed parameters and superior in precision and recall compared to existing analytical models.

Upon assessment of the accuracy and robustness of the proposed RAMD model, the large dataset (two-month period) was processed for DZ analysis using the framework presented in Figure 4. The final dataset contained the features at advance and stop-bar detectors for the match pairs predicted by the RAMD model. The travel time between the advance and stop-bar detector can now be estimated for a matching pair as the difference of timestamps at which the actuation was 'on' at the stop-bar and advance locations. We conducted a detailed empirical assessment of Type I and Type II DZ based on this estimated travel time and the stop/run decision for a matching pair based on the SCA parameter.

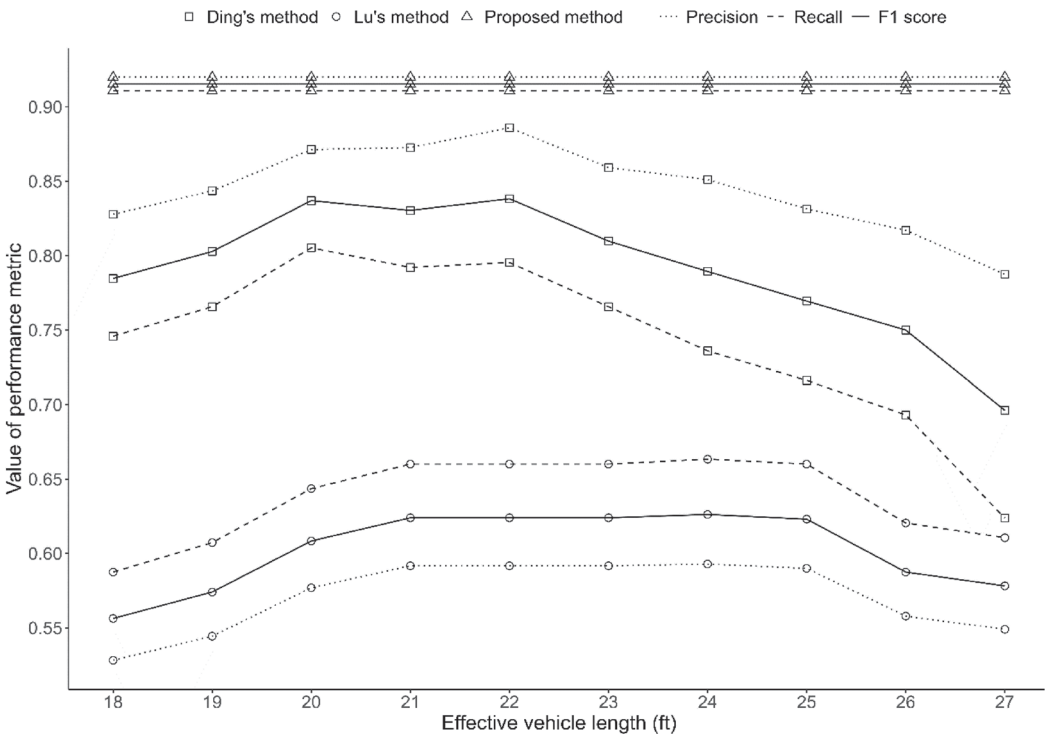

Figure 5. Performance comparison of Ding's and Lu's method with the proposed RAMD model.

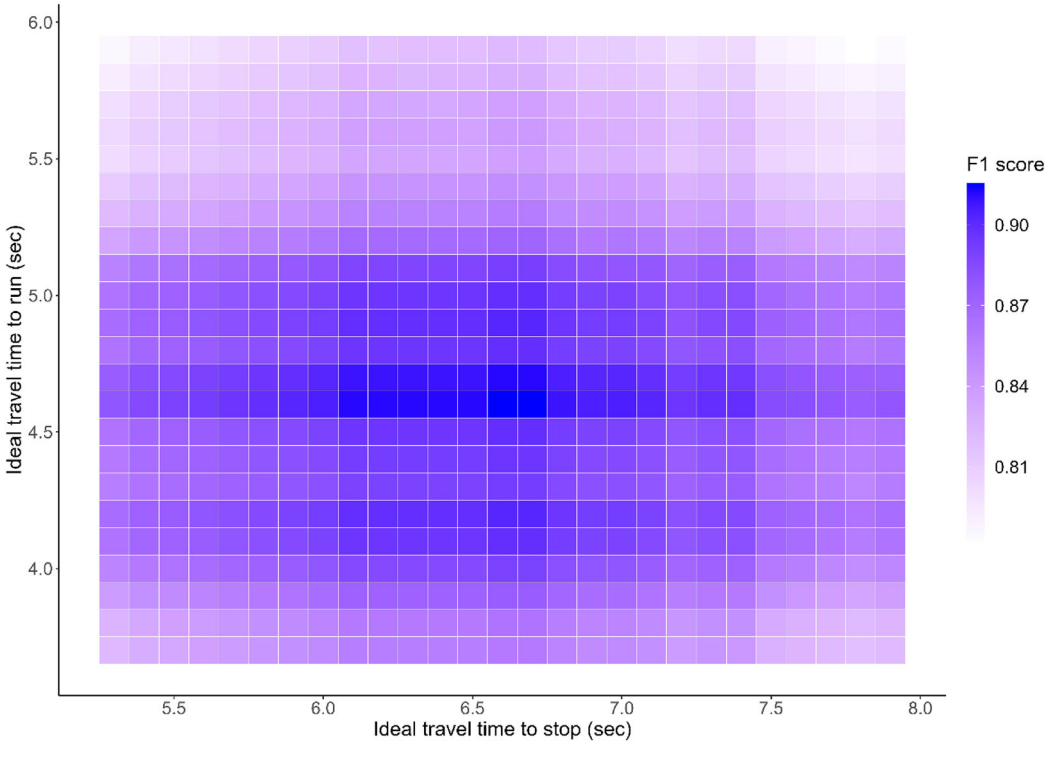

Figure 6. Sensitivity analysis of the proposed RAMD model.

Dilemma zone analysis

Type I DZ and Option Zone

We subjectively define the 'approach' of the intersection as the road space between the stop-bar and advance detector locations. The approach velocity of a vehicle (V_i) can then be computed based on the time taken to traverse the distance between the advance and stop-bar detectors (t_i), as shown in Eq. (6). Recall that this travel time is output from processing the dataset for the matching pairs obtained from the RAMD model.

$$V_i = \frac{D'}{t_i} \qquad \forall i \tag{6}$$

With approach velocity known, the vehicle's position from the stop line at the yellow onset can be accurately estimated based on whether the vehicle arrived at the advance and stop-bar locations before or after the indication turned yellow. At the yellow onset, a vehicle's position can be in one of three areas: (a) between the stop line and the end of the stop-bar detector, (b) between the stop-bar and advance detectors, and (c) beyond the advance detector. A vehicle's position in an area can be identified based on each detector's AIY and TUY parameters. In the matched dataset, $AIY_i < TUY_i$ indicates vehicle i's arrival at the advance location after the indication turns yellow, implying that the vehicle's position is beyond the advance detector. On the other hand, $AIY_i > TUY_i$ implies vehicle i's arrival at the advance location before the indication turns yellow, so two further cases are possible here. $AIY_i' < TUY_i'$ indicates arrival at the stop-bar after the indication turns yellow, implying that the vehicle's position is between the stop-bar and advance detectors. $AIY_i' > TUY_i'$ indicates that the vehicle arrives at the stop-bar before the indication turns yellow, implying that the vehicle's position is between the stop line and the end of the stop-bar detector. (A negative value of the vehicle's position implies that the front of the vehicle has crossed the stop line.) Based on the conditions mentioned above, vehicle i's position at the onset of yellow, X_i^p, for the three areas can be computed using Eq. (7).

$$X_i^p = \begin{cases} D + AIY_i * V_i, & AIY_i < TUY_i \qquad \forall i \\ d + AIY_i^{'} * V_i, & AIY_i > TUY_i, AIY_i^{'} < TUY_i^{'} \qquad \forall i \\ d - TUY_i^{'} * V_i, & AIY_i > TUY_i, AIY_i^{'} > TUY_i^{'} \qquad \forall i \end{cases} \tag{7}$$

Besides X_i^p, the estimation of Type I DZ and option zone depend on the minimum stopping distance (X_i^s) and the maximum clearing distance (X_i^c) for each vehicle. Computation of X_i^s and X_i^c necessitates estimation of the GHM model parameters: the minimum perception-reaction time, the maximum deceleration rate for stopping vehicles, and the maximum acceleration rate for running vehicles. We estimate these parameters for each vehicle based on the findings of Wei et al. (2011), where the authors calibrated and modified the GHM model parameters based on empirical assessment of vehicle trajectory data. Eq. (8), (9), and (10) summarize the calibrated values proposed by Wei et al. (2011) for estimating the minimum perception reaction time (δ_i), the maximum deceleration rate for stopping vehicles a_i^{stop}, and the maximum acceleration rate for running vehicles a_i^{run}. Note that the parameters are calibrated as functions of approach velocity of individual vehicle (V_i) and the 85th percentile speed of intersection's approach (V_{85}). Interested readers are referred to Wei et al. (2011) for details on the calibration of the GHM model parameters. The 85th percentile speed for the westbound approach was obtained using INRIX data. INRIX provides minute-by-minute timestamps of speed and travel time on road segments. All speed data for January and February was collected, the analysis of which yielded 38 mph (61 km/hr) as the 85th percentile speed on the intersection approach.

$$\delta_i(V_i) = 0.445 + \frac{21.478}{V_i} \qquad \forall i \tag{8}$$

$$a_i^{stop}(V_i, V_{85}) = \exp\left(3.379 + \frac{-36.099}{V_i}\right) - 9.722 + \frac{429.692}{V_{85}} \qquad \forall i \tag{9}$$

$$a_i^{run}(V_i, V_{85}) = -27.91 + \frac{760.258}{V_i} + 0.266 * V_{85} \qquad \forall i \tag{10}$$

Let $\alpha_i \in \{0, 1\}$ be a binary variable representing the decision of vehicle i to either stop at ($\alpha_i = 0$) or run over ($\alpha_i = 1$) the intersection stop line, as shown in Eq. (11). Following assumptions in Wei et al. (2011), we assume that the minimum perception reaction time is equal for stopping and running vehicles. In estimation of X_i^s and X_i^c, note that the GHM model parameters calibrated by Wei et al. (2011) do not explicitly define the limits on the deceleration rate for running vehicles and the acceleration rate for stopping vehicles. Based on the assumptions in prior literature, we limit the maximum deceleration rate for running vehicles (a_{crit}^{stop}) to 10 ft/s^2 (Ding et al. 2016; Lu et al. 2015; Chen et al. 2021) and the maximum acceleration for stopping vehicles (a_{crit}^{run}) to 6 ft/s^2 (Long 2000). With the assumptions above and the knowledge of the GHM model parameters, X_i^s and X_i^c can be computed using Eq. (12) and (13), respectively.

$$\alpha_i = \begin{cases} 0, & SCA_i^{'} \in \{RG\} \\ 1, & otherwise \end{cases} \qquad \forall i \tag{11}$$

$$X_i^s = \begin{cases} V_i * \delta_i + \dfrac{V_i^2}{2 * a_i^{stop}}, & \alpha_i = 0 \\ V_i * \delta_i + \dfrac{V_i^2}{2 * a_{crit}^{stop}}, & \alpha_i = 1 \end{cases} \qquad \forall i \tag{12}$$

$$X_i^c = \begin{cases} V_i * \gamma + 0.5 * a_i^{run} * (\gamma - \delta_i)^2, & \alpha_i = 1 \\ V_i * \gamma + 0.5 * a_{crit}^{run} * (\gamma - \delta_i)^2, & \alpha_i = 0 \end{cases} \qquad \forall i \tag{13}$$

With X_i^p, X_i^s, and X_i^c computed, we can identify if vehicle i is in a specific zone based on the following rules (Lu et al. 2015):

1. In should-go zone: if $X_i^p \le X_i^c \le X_i^s$ or $X_i^p \le X_i^s \le X_i^c$
2. In should-stop zone: if $X_i^p \ge X_i^c \ge X_i^s$ or $X_i^p \ge X_i^s \ge X_i^c$
3. In Type I dilemma zone: if $X_i^c < X_i^p < X_i^s$
4. In option zone: if $X_i^s < X_i^p < X_i^c$

The Type I DZ begins at X_i^s and ends at X_i^c, whereas the option zone starts at X_i^c and ends at X_i^s. For a dynamic analysis of Type I DZ and option zone, the time of day for each actuation was discretized into four groups: morning (5 am – 9 am), mid-day (9 am – 3 pm), evening peak (3 pm – 7 pm), and overnight (7 pm – 5 am). Also, the days of the week were divided into two groups: weekdays and weekends (including public holidays).

Type II DZ

Given the definitions and rule-of-thumb in the transportation literature for Type II DZ, we sought its empirical analysis through probabilistic and travel time-based methods. Recall that the probabilistic approach defines Type II DZ as the approach area where more than 10% and less than 90% of vehicles opt to stop at yellow onset. Similarly, the widely adopted rule-of-thumb in light of the travel time-based approach demarcates Type II DZ as an indecision zone between 2.5 and 5.5 sec upstream of the intersection at yellow onset. With X_i^p computed in the earlier section, the Type II DZ can be estimated for varying approach velocities and time of day. Each hour's Type II DZ boundary dynamics can be estimated based on the 10th and 90th percentiles of vehicles stopping. Since only vehicles approaching

the intersection up to a certain velocity would stop at the stop line, the dynamics of Type II DZ boundary by approach velocity differs for the probabilistic and travel time-based approaches, as presented in the results section.

Results and discussions

This section discusses the findings for DZ parameters and boundaries based on Type I and Type II definitions.

Type I DZ parameters

At yellow onset, driving characteristics–namely approach velocity, perception reaction time, acceleration, and deceleration–were estimated using Equations (6), (8), (9), and (10), respectively. Table 5 summarizes the descriptive statistics of these Type I DZ parameters.

The mean and median of approach velocity at the onset of yellow were equal to the speed limit of the approach. The mean perception reaction time was 0.89 sec, compared to 1.0 and 1.5 sec assumed by ITE's traffic engineering handbook (ITE 1999) and AASHTO (Click 2008), respectively. Negative values for the acceleration of the running vehicles indicate that drivers apply some decelerating force for safety purposes when crossing the intersection at yellow onset. The mean and median acceleration values were around 0 ft/s^2, parallel to the assumptions in ITE and AASHTO. The maximum acceleration observed was 5.34 ft/s^2, which is still lower than the maximum acceleration limit of 6 ft/s^2 proposed by Long (2000). The mean and median deceleration of stopping vehicles were 9.82 and 9.89 ft/s^2, respectively. The ITE and AASHTO assume maximum deceleration rates of 10 and 11.2 ft/s^2, respectively. Overall, the descriptive statistics of Type I DZ parameters demonstrate a realistic estimation of these parameters using the calibration models proposed by Wei et al. (2011).

Type I decision rule vs. actual decision taken

As discussed in the previous section, the Type I decision rule dictates whether the vehicle is in a should-stop, should-go, dilemma, or option zone based on the values of X_i^p, X_i^s, and X_i^c. Of the total sample size of 28,700 vehicles, we observed 1,042 vehicles in DZ and 348 in the option zone, indicating 4.8% of vehicles in either of the two zones at yellow onset. An interesting observation here is the number of vehicles in the should-stop zone that decided to run through the intersection stop line. These 2,386 vehicles account for 8.3% of vehicle arrivals at yellow onset that should have stopped, but they either cannot make a stop or drive past the stop line anyway owing to the inherent driving behavior. Since 8.3% is a significant portion of vehicle arrivals at yellow onset, we hypothesize that the dilemma zone protection might not be adequate at the site's approach.

Recall that the stop/run decision for an actuation over the stop bar detector was accurately identified using a combination of signal change during actuation and occupancy time parameters during

Table 5. Summary of driving characteristics at yellow onset

Parameters	Approach velocity (mph)	Perception reaction time (sec)	Acceleration of running vehicles (ft/s^2)	Deceleration of stopping vehicles (ft/s^2)
Sample size	28,700	28,700	16,281	12,419
min	16.00	0.69	−4.30	4.36
5th percentile	22.00	0.74	−3.14	6.88
25th percentile	28.00	0.79	−1.68	8.79
median	35.00	0.87	−0.51	9.89
mean	35.23	0.89	−0.24	9.82
75th percentile	42.00	0.97	0.95	10.92
95th percentile	49.00	1.10	3.00	12.44
max	59.00	1.35	5.34	13.70

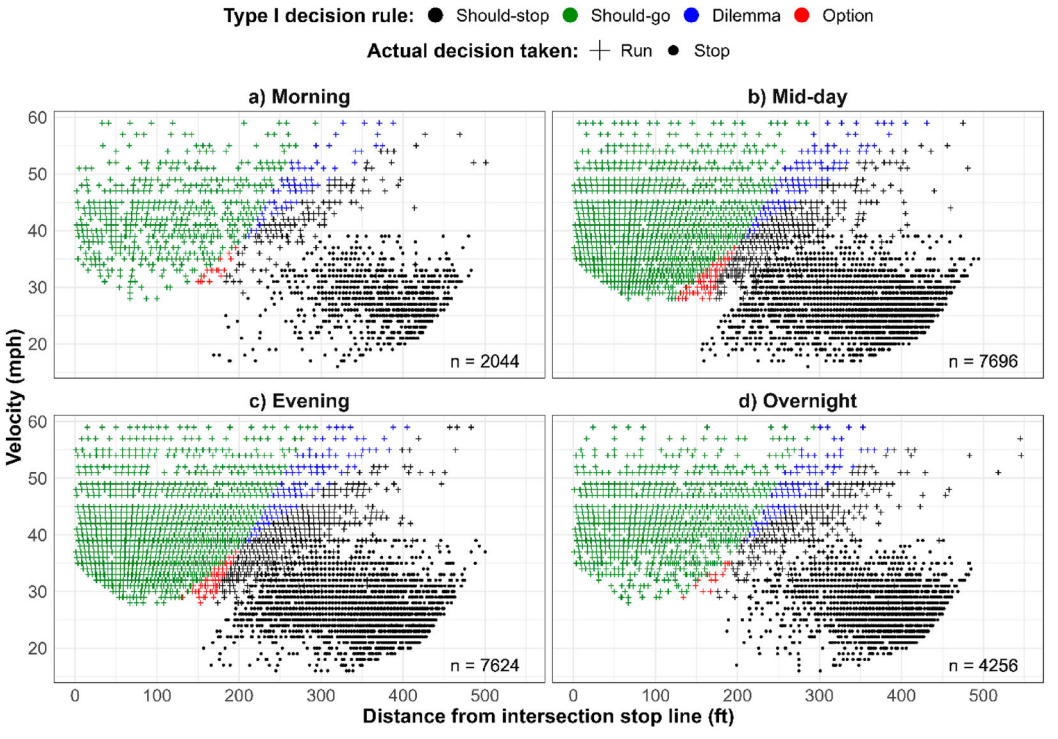

Figure 7. Type I decision rule vs. actual decision taken (weekdays).

data processing. This stop bar actuation, when matched with an advance actuation using the proposed RAMD model, yielded a match-paired vehicle's actual stop/run decision at the intersection. Figure 7 depicts the variation of the Type I decision rule vs. actual stop/run decision taken by approach velocity and time of day categories for weekdays; Figure 8 presents the same for weekends. A vehicle's stop or run decision while approaching the intersection depends on the approach velocity and the vehicle's position from the intersection stop line. Vehicles that encounter the yellow onset near the intersection stop line tend to cross the intersection at a higher approach speed. On the other hand, most vehicles that encounter the yellow onset far from the intersection stop line reduce their approach speed to stop safely before the intersection stop line. Furthermore, irrespective of the time of day and weekday/weekend, there is a combination of an approach velocity and a vehicle's distance from the intersection stop line that separates vehicles falling into DZ (in blue) and option zone (in red). For instance, in Figure 7(c), the dilemma and option zones are separated on the x-axis at approximately 200 ft and the y-axis at approximately 38 mph (61 km/hr).

The ideal case where vehicles make the correct stop/run decision per the rules of Type I definition accounts for 86.8%. Within these two ideal cases are the remaining 13.2% of vehicle arrivals that can be categorized into three: DZ (in blue), option zone (in red), and vehicles taking Type I-contrary stop/run decisions (in black marked '+'). Ideally, the DZ protection system should be targeted to these three categories where vehicles are susceptible to either being trapped in an indecision zone or making Type I-contrary stop/run decisions.

Variation of dilemma zone boundaries by hour

Figure 9 presents how the Type I DZ, the option zone, the Type II probabilistic DZ, and the Type II travel time-based DZ vary along different hours of the day. The DZ boundaries defined by the Type I and Type II definitions differ significantly. Compared to its end, the start of the Type II probabilistic

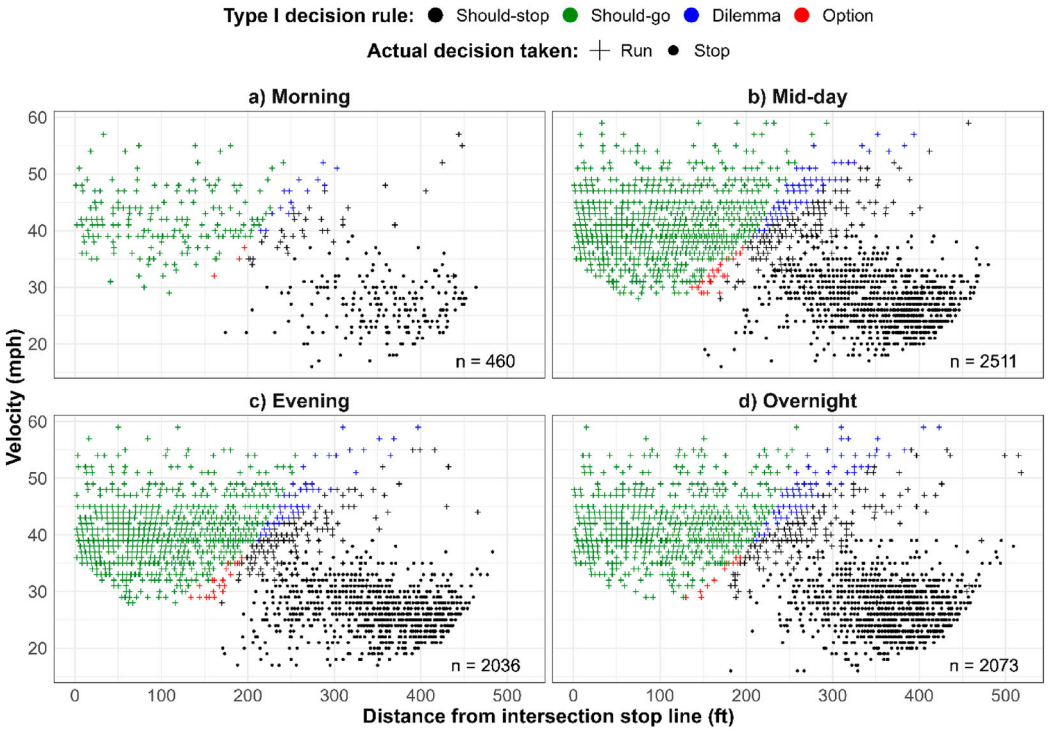

Figure 8. Type I decision rule vs. actual decision taken (weekends).

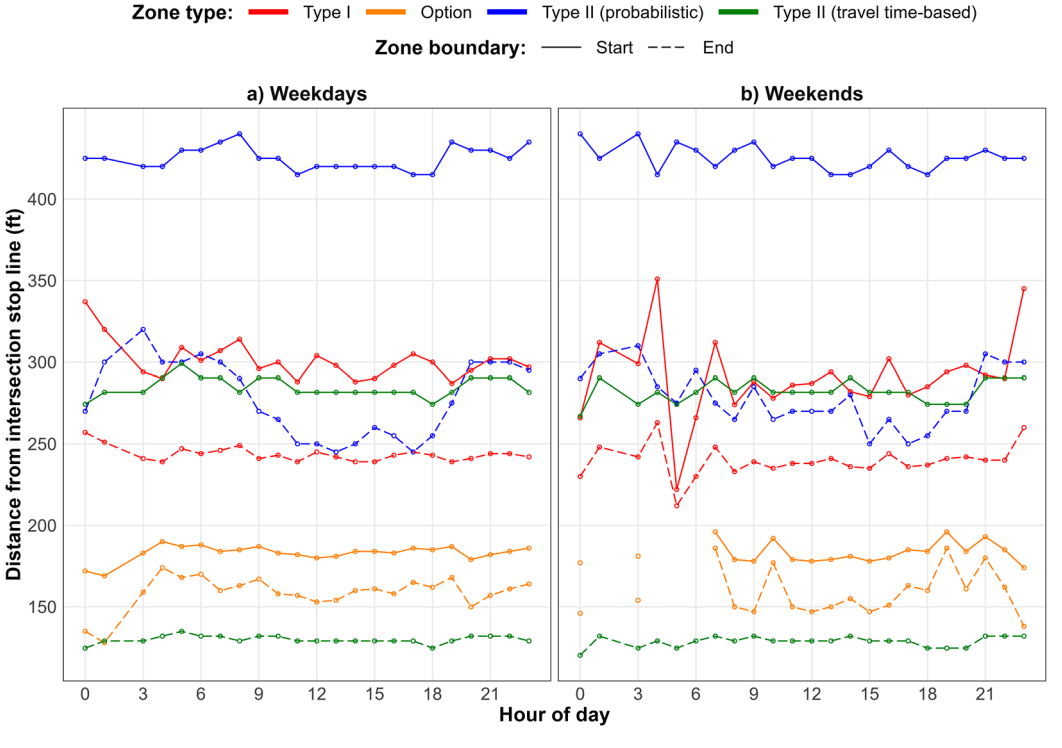

Figure 9. Variation of dilemma zone boundaries by hour for weekdays and weekends.

DZ (in blue) does not fluctuate much by hour over both weekdays and weekends. Further, this boundary increases during the day, especially during the evening peak. The Type II travel time-based DZ's boundary (in green) does not fluctuate much temporally. Notice that the probabilistic and travel time-based definitions of Type II DZ do not overlap. Instead, there is always a margin separating the two boundaries. Moreover, the probabilistic boundary is far from the intersection stop line compared to the travel time-based DZ boundary.

The option zone from the Type I definition is enclosed within the Type II travel time-based DZ boundary. The option zone (in orange) is located near the intersection stop line, which intuitively makes sense as we observed from Figure 7 and Figure 8 that the option zone is: (a) located close to the stop line; (b) is created at lower approach velocity, and (c) is of shorter boundary length. Also, note that the end of the option zone, compared to the start, fluctuates more over different hours. The Type I DZ (in red) fluctuates more on weekends than weekdays and is explicitly separated from the option zone. The overlap of Type I DZ with the probabilistic boundary shows that the latter provides some protection for Type I DZ.

Variation of dilemma zone boundaries by approach velocity

Figure 10 presents the variation of different DZ boundaries by approach velocity, overlaid on top of the Type I decision rule and the actual decision taken by drivers. Each observation in this figure indicates an approaching vehicle with its velocity and distance from the intersection stop line at the yellow onset. The colors represent the Type I decision rule, while the symbols indicate the actual decision taken by drivers. For instance, an observation labeled by a black 'plus' represents a vehicle deciding to cross the intersection while the Type I decision rule dictated that the vehicle should stop; an observation labeled by a blue 'plus' represents a vehicle deciding to cross the intersection while being in a Type I

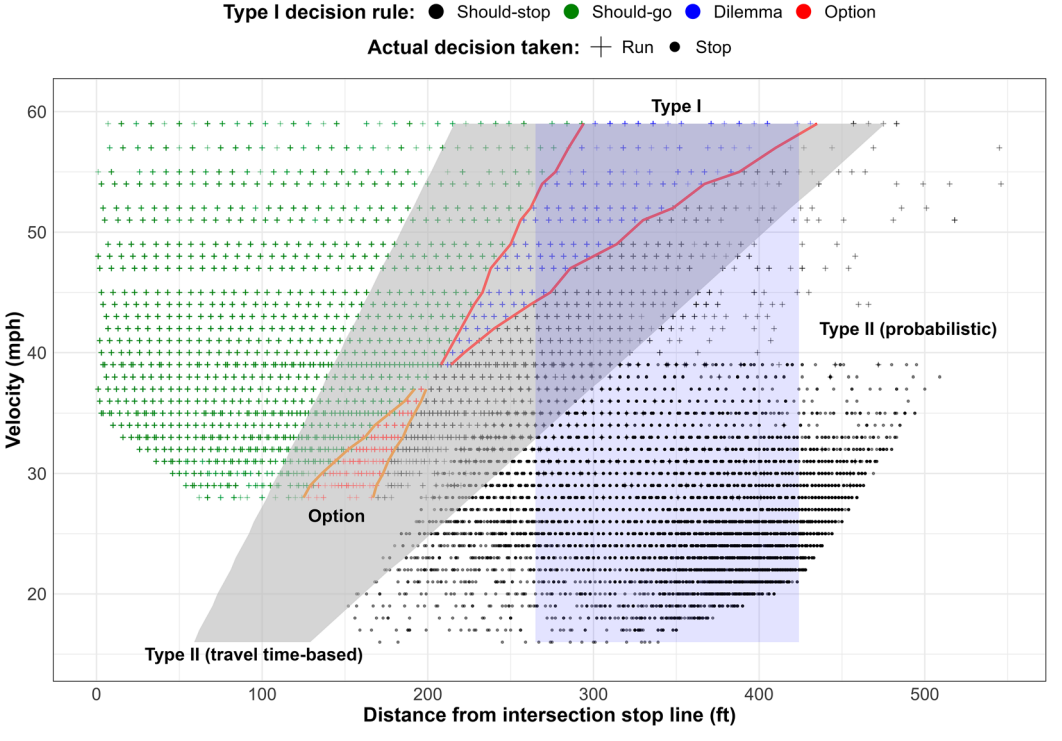

Figure 10. Variation of dilemma zone boundaries by approach velocity.

DZ; similarly, an observation labeled by a black 'dot' represents a vehicle that stopped before the stop line while the Type I decision rule also dictated that the vehicle should stop. Furthermore, the Type I DZ, option zone, Type II probabilistic DZ, and Type II travel time-based DZ are demarcated by their respective boundaries in Figure 10.

We observe that the start and end boundaries of Type I DZ are dictated explicitly by vehicles in DZ. A similar case is observed for the option zone. The Type I DZ boundary is wider at higher approach velocity and narrower at lower approach velocity. The Type I dilemma and option zones converge and tend to meet at a velocity of 38 mph (61 km/hr). This virtual point was the 85th percentile speed observed from the analysis of INRIX data for two months. Note the vehicles arriving above or below this velocity limit and making the wrong decision (in black with '+'). We observe that neither the Type I DZ nor the option zone protects these vehicles from making Type I-contrary decisions.

The Type II probabilistic DZ is constant and does not vary by approach speed, drawing a parallel to the findings of Rahman, Kang, and Biswas (2021). It extends from 265 ft (80.8 m) to 425 ft (129.5 m), failing to protect vehicles in the indecision zone and vehicles making Type I-contrary decisions outside the boundary. The Type II travel time-based counterpart, on the other hand, is a linear function of approach velocity. With a wider zone boundary for higher approach speed, it also fails to provide DZ protection to all vehicles in Type I-contrary decision zones. While Type II travel time-based and Type II probabilistic DZ did not overlap by the time of day (refer Figure 9), there is some overlap between the two when we account for the variation by approach velocity.

Note that the vehicles in the Type I DZ (in blue), in the option zone (in orange), and making the Type I-contrary decision (in black marked '+') are the ones in need of DZ protection at an intersection approach. The integrated empirical analysis of both Type I and Type II definitions presented in this study shows that none of the existing definitions are consistent in providing satisfactory protection to vehicles approaching with either 'indecision' or 'Type I-contrary decision' at yellow onset. Our findings demonstrate the need for more empirical analysis and novel data-driven dynamic models of DZ boundary, which varies by approach speed, hourly volume, and time of day.

Practical implications

The analyses and findings in this study have significant implications for several stakeholders, including traffic engineers and vehicle manufacturers. Traffic engineers could consider the dynamic nature of DZ boundary in developing optimal strategies for signal control and advance detector placement. Moreover, the importance of accurate quantification and demarcation of DZ boundary–emphasized by this study's findings–enables traffic engineers to understand drivers' stop/go behavior and develop proactive measures for mitigating red light running tendencies at signalized intersections. Similarly, vehicle manufacturers and autonomous driving technology developers can consider the dynamics of DZ boundaries to refine vehicle control algorithms and ensure safer decision-making in response to the safety-critical yellow onset periods. At a broader level, this study's findings highlight the need to further investigate the dynamics of DZ boundary, especially using data obtained from advanced detection sensors such as radars and LiDARs; data from such sensors could potentially provide accurate estimates of Type I DZ parameters for predicting and mitigating DZ-related risks in real-time.

While this study offers novel insights and a detailed empirical analysis of DZ using a large sample size, it also opens avenues for future research to address its limitations and constraints. The ground-truth values of the Type I DZ parameters are difficult to obtain with non-visual high-resolution event data from loop detectors. As a result, this study used the empirical models proposed by Wei et al. (2011) to estimate the Type I DZ parameters. Ground-truth values of these parameters could be obtained by setting up cameras upstream of the intersection approach (Wei et al. 2011) and using either manual or computer vision-based tracking. Future research could implement such a setup and test the accuracy of estimating Type I DZ parameters using data from connected vehicles or advanced detection sensors such as LiDAR. Also, the matching methodology proposed in this study only considered lane changes to the left-turn lane but not on the through lanes. Manual observation of 7 hours of ground-truth

videos showed that only 2% of vehicles changed lanes on the through lane during the yellow onset. With regard to DZ boundary quantification, impacts of weather conditions, presence of non-motorized users, and driver behavior changes over time are additional factors that could be covered in future research.

Conclusions

This study empirically assessed the existing approach and definitions used to quantify DZ in an intersection approach. The potential overlap between Type I and Type II DZ boundaries and their integrated empirical assessment was identified as a research gap, the exploration of which would contribute better to our understanding of DZ. To this end, we processed high-resolution event data for two months and proposed a novel rule-based methodology to match actuation events between the advance and stop-bar detector locations. The proposed matching method had an accuracy of 92% and a recall of 91%. Performance comparison with two existing analytical matching methodologies in the literature showed that the proposed matching method is more accurate and robust to the assumption of deterministic parameters such as effective vehicle length.

The matching methodology was applied to process a large dataset of high-resolution detector actuation events to obtain 28,700 samples of vehicle arrivals at the yellow onset. An empirical exploratory analysis of the Type I DZ, the option zone, the Type II probabilistic DZ, and the Type II travel time-based DZ led to some novel, insightful findings, which are summarized as follows:

- 86.8% of vehicles make the correct stop/run decisions per the Type I rules. The rest, 13.2% of vehicles, either fall into an indecision zone or make a Type I-contrary stop/run decision at the intersection approach. An efficient DZ protection system should reduce the proportion of vehicles failing into 'indecision' and 'Type I-contrary decision' zones.
- The boundaries of the Type I DZ and the option zone did not fluctuate much by the time of day and hour. The Type II probabilistic DZ boundary increases during the day, especially the evening peak, while the travel time-based boundary does not vary much with time of day.
- The probabilistic and travel time-based boundaries of Type II DZ overlap only at higher approach velocity. Similarly, the Type I DZ and the option zone boundaries do not overlap. The Type I DZ boundary does overlap with the Type II probabilistic DZ boundary, indicating that the latter provides some protection for DZ defined based on the minimum stopping distance and the maximum clearing distance.
- The Type I DZ boundary is wider at higher approach velocity. Neither of the Type I zones protects vehicles making Type I-contrary decisions. The Type II probabilistic DZ does not vary by approach velocity. It and the travel time-based DZ fail to fully protect vehicles in the 'indecision' and 'Type I-contrary decision' zones.

Our empirical analysis concluded that none of the existing definitions of DZ are consistent in providing satisfactory protection to vehicles approaching the intersection in either 'indecision' or 'Type I-contrary decision' zones. This novel finding underscores the need for further detailed empirical analysis of vehicle arrivals and dynamic DZ boundary models that vary by approach speed, hourly volume, and time of day. Given the analyses and findings of this study, there is a significant research prospect in using machine learning methods and big data from advanced detection sensors or connected vehicles to assess DZ boundary in real-time. Such an approach will provide a detailed assessment of the relatively understudied insights on the dynamics and accurate quantification of dilemma zone boundary.

Acknowledgments

The authors thank the City of Phoenix for partial funding of this study. The authors also thank Simon Ramos, Robert Kyser, and Eric Hernandez for facilitating this study's VPN access, data access, and video recordings. Special thanks to Cristina

Valencia Reyes and Will Reuter for assistance with manually verifying detection matches from videos. Comments from anonymous referees led to substantial improvements in the manuscript.

Disclosure statement

No potential conflict of interest was reported by the author(s).

ORCID

Pramesh Pudasaini http://orcid.org/0000-0002-4238-1097

References

Bonneson, James, Dan Middleton, Karl Zimmerman, Hassan Charara, and Montasir Abbas. 2002. *Intelligent Detection-Control System for Rural Signalized Intersections*. Texas Department of Transportation.

Brackstone, Mark, and Mike McDonald. 1999. "Car-following: A Historical Review." *Transportation Research Part F: Traffic Psychology and Behaviour* 2 (4): 181–196. https://doi.org/10.1016/S1369-8478(00)00005-X

Chang, Myung-Soon, Carroll J Messer, and Alberto J Santiago. 1985. "Timing Traffic Signal Change Intervals Based on Driver Behavior." *Transportation Research Record* 1027:20-30.

Chen, Peng, Lei Wei, Fangfang Meng, and Nan Zheng. 2021. "Vehicle Trajectory Reconstruction for Signalized Intersections: A Hybrid Approach Integrating Kalman Filtering and Variational Theory." *Transportmetrica B: Transport Dynamics* 9 (1): 22–41. https://doi.org/10.1080/21680566.2020.1781707

Chen, Peng, Guizhen Yu, Xinkai Wu, Yilong Ren, and Yueguang Li. 2017. "Estimation of red-Light Running Frequency Using High-Resolution Traffic and Signal Data." *Accident Analysis & Prevention* 102: 235–247. https://doi.org/10.1016/j.aap.2017.03.010

Click, Steven M. 2008. "Application of the ITE Change and Clearance Interval Formulas in North Carolina." *Institute of Transportation Engineers. ITE Journal* 78 (1): 20.

Ding, Chuan, Xinkai Wu, Guizhen Yu, and Yunpeng Wang. 2016. "A Gradient Boosting Logit Model to Investigate Driver's Stop-or-run Behavior at Signalized Intersections Using High-Resolution Traffic Data." *Transportation Research Part C: Emerging Technologies* 72: 225–238. https://doi.org/10.1016/j.trc.2016.09.016

Gates, Timothy J, and David A Noyce. 2010. "Dilemma Zone Driver Behavior as a Function of Vehicle Type, Time of day, and Platooning." *Transportation Research Record: Journal of the Transportation Research Board* 2149 (1): 84–93. https://doi.org/10.3141/2149-10

Gazis, Denos, Robert Herman, and Alexei Maradudin. 1960. "The Problem of the Amber Signal Light in Traffic Flow." *Operations Research* 8 (1): 112–132. https://doi.org/10.1287/opre.8.1.112

Hurwitz, David S, Haizhong Wang, Michael A Knodler, Daiheng Ni, and Derek Moore. 2012. "Fuzzy Sets to Describe Driver Behavior in the Dilemma Zone of High-Speed Signalized Intersections." *Transportation Research Part F: Traffic Psychology and Behaviour* 15 (2):132-143. https://doi.org/10.1016/j.trf.2011.11.003

ITE. 1999. "Traffic Engineering Handbook." In.: *ITE* Washington, DC.

Jalali Khalilabadi, Pouya, Abolfazl Karimpour, and Yao-Jan Wu. 2023. "Severity Analysis of red-Light–Running Behavior at Signalized Intersections." *Journal of Transportation Safety & Security*: 1-25.

Kang, Min-Wook, Moynur Rahman, and Joyoung Lee. 2020. "Determination and Utilization of Dilemma Zone Length and Location for Safety Assessment of Rural High-Speed Signalized Intersections." *Transportation Research Record: Journal of the Transportation Research Board* 2674 (4): 272–280. https://doi.org/10.1177/0361198120911929

Karimpour, Abolfazl, Jason C Anderson, Sirisha Kothuri, and Yao-Jan Wu. 2022. "Estimating Pedestrian Delay at Signalized Intersections Using High-Resolution Event-Based Data: A Finite Mixture Modeling Method." *Journal of Intelligent Transportation Systems* 26 (5): 511–528. https://doi.org/10.1080/15472450.2021.1926246

Li, Xiaofeng, and Yao-Jan Wu. 2021. "Real-time Estimation of Pedestrian Volume at Button-Activated Midblock Crosswalks Using Traffic Controller Event-Based Data." *Transportation Research Part C: Emerging Technologies* 122: 102876. https://doi.org/10.1016/j.trc.2020.102876

Long, Gary. 2000. "Acceleration Characteristics of Starting Vehicles." *Transportation Research Record: Journal of the Transportation Research Board* 1737 (1): 58–70. https://doi.org/10.3141/1737-08

Lu, Guangquan, Yunpeng Wang, Xinkai Wu, and Henry X Liu. 2015. "Analysis of Yellow-Light Running at Signalized Intersections Using High-Resolution Traffic Data." *Transportation Research Part A: Policy and Practice* 73: 39–52. https://doi.org/10.1016/j.tra.2015.01.001

National Academies of Sciences, Engineering, and Medicine. 2012. "Guidelines for Timing Yellow and All-Red Intervals at Signalized Intersections."

Papaioannou, Panagiotis. 2007. "Driver Behaviour, Dilemma Zone and Safety Effects at Urban Signalised Intersections in Greece." *Accident Analysis & Prevention* 39 (1): 147–158. https://doi.org/10.1016/j.aap.2006.06.014

Pudasaini, Pramesh, Abolfazl Karimpour, and Yao-Jan Wu. 2023. "Real-Time Queue Length Estimation for Signalized Intersections Using Single-Channel Advance Detector Data." *Transportation Research Record: Journal of the Transportation Research Board* 2677 (7): 144–156. https://doi.org/10.1177/03611981221151066

Rahman, Moynur, Min-Wook Kang, and Pranesh Biswas. 2021. "Predicting Time-Varying, Speed-Varying Dilemma Zones Using Machine Learning and Continuous Vehicle Tracking." *Transportation Research Part C: Emerging Technologies* 130: 103310. https://doi.org/10.1016/j.trc.2021.103310

Ren, Yilong, Yunpeng Wang, Xinkai Wu, Guizhen Yu, and Chuan Ding. 2016. "Influential Factors of red-Light Running at Signalized Intersection and Prediction Using a Rare Events Logistic Regression Model." *Accident Analysis & Prevention* 95: 266–273. https://doi.org/10.1016/j.aap.2016.07.017

Savolainen, Peter T, Anuj Sharma, and Timothy J Gates. 2016. "Driver Decision-Making in the Dilemma Zone – Examining the Influences of Clearance Intervals, Enforcement Cameras and the Provision of Advance Warning Through a Panel Data Random Parameters Probit Model" *Accident Analysis & Prevention* 96: 351–360. https://doi.org/10.1016/j.aap.2015.08.020

Sharma, Anuj, Darcy Bullock, and Srinivas Peeta. 2011. "Estimating Dilemma Zone Hazard Function at High Speed Isolated Intersection." *Transportation Research Part C: Emerging Technologies* 19 (3): 400–412. https://doi.org/10.1016/j.trc.2010.05.002

Urbanik, Tom, and Peter Koonce. 2007. "The Dilemma with Dilemma Zones." *Proceedings of ITE District 6*.

Wei, Heng, Zhixia Li, Ping Yi, and Kevin R Duemmel. 2011. "Quantifying Dynamic Factors Contributing to Dilemma Zone at High-Speed Signalized Intersections." *Transportation Research Record: Journal of the Transportation Research Board* 2259 (1): 202–212. https://doi.org/10.3141/2259-19

Wu, Xinkai, Natanael D Vall, Henry X Liu, Wen Cheng, and Xudong Jia. 2013. "Analysis of Drivers' Stop-or-run Behavior at Signalized Intersections with High-Resolution Traffic and Signal Event Data." *Transportation Research Record: Journal of the Transportation Research Board* 2365 (1):99-108. https://doi.org/10.3141/2365-13

Zegeer, Charles V, and Robert Curba Deen. 1978. *Green-extension Systems at High-Speed Intersections*. Vol. 496: Citeseer.

Zhang, Yaping, Chuanyun Fu, and Liwei Hu. 2014. "Yellow Light Dilemma Zone Researches: A Review." *Journal of Traffic and Transportation Engineering (English Edition)* 1 (5): 338-352.